Lab on a Chip

Accepted Manuscript

ROYAL SOCIETY OF CHEMISTRY

www.rsc.org/loc

Lab on a Chip

RSCPublishing

ARTICLE

Fast and cost-effective fabrication of large-area plasmonic transparent biosensor array

Cite this: DOI: 10.1039/x0xx00000x

R. Intartaglia,[a]* S. Beke,[a] M. Moretti,[b] F. De Angelis,[b] and A. Diaspro,[a]

Received 00th January 0000,
Accepted 00th January 0000

DOI: 10.1039/x0xx00000x

www.rsc.org/

Surface Enhanced Raman-based sensors are widely used for chemical and biological specie analysis, but to date the high cost, long production time, hazardous, and toxic content with small sensing area and opacity are limiting their capabilities for widespread applications in the medical and environmental fields. We present a novel cost-effective method for fast laser-based fabrication of affordable large-area and transparent periodic arrays of ligand-free metallic nanoparticles, offering a maximum possibility for the adsorption/immobilization of molecules and labeling. Further, we demonstrate a remarkable detection limit in the picomolar range by means of Raman Scattering, thus evidencing a superior signal-to-noise ratio compared to other sensor substrates. The high sensitivity performance together with a fast and cheap fabrication procedure of reusable large-area transparent plasmonic devices open the route for direct, *in situ* multimodal optical analysis with broad applications in the biomedical/analytical fields.

Introduction

Plasmonics is becoming a driving force in the development of various optical devices with broad applications in the fields of biology, chemistry, biosensor, and recently in the development of future solar cells.[1-3] Due to the unique interaction of light with the free surface electrons in the metal nanostructure, known as plasmon resonance, such metallic particles have extremely high scattering and absorption cross-sections. Thus, the local electromagnetic field of incoming light can be remarkably enhanced.[4, 5] These phenomena enable metal nanoparticles (NPs) to serve as a plasmonic light trapping for thin-film solar cell devices, intense labels for immunoassays[6-8] , biochemical sensors[9-14] , and surface-enhanced spectroscopies[15-22]. Among these applications, Surface Enhanced Raman Spectroscopy (SERS) is a highly efficient analytical tool applied in the medical field to study the trace analytes (e.g., urea, citric acid) and chemical changes in blood and urine[23, 24] and for the detection of mercury (II) ions in drinking water[25].

During the past decades, researchers have made great efforts to find ideal SERS substrates, mainly including pioneering works on the preparation of metal nanostructure arrays by various methods[26-34], such as template-based method[35], electron beam lithography[26-28], optical lithography[29], pulsed laser lithography[30-34], and hazardous and toxic metallic nano-objects deposition on surfaces[36]. These techniques present some limitations or drawbacks, such as high cost, long production time and critical SERS detection. The SERS detection is mainly limited due to the presence of artificial ligand on the chemically synthesized nanoparticles and/or chemical linkers to immobilize nanoparticles on SERS substrate[37]. Another limitation concerns the opacity of these SERS substrates to visible light, which impedes the visualization of the microscopic details of the biological substances. In this context, much effort is currently being put in the development of transparent SERS devices, which will open up opportunities for more challenging applications, such as direct, non-invasive and online multimodal optical analyses, i.e. simultaneous optical examination of specific biological samples and their SERS characterizations in various states. Despite some approaches that are available to make SERS devices transparent, such as low temperature oblique angle deposition[38] and ion drift process[39], this issue still represents a limitation in this field.

Here we present a comparatively simple approach for the realization of cheap and large-area hydrophobic transparent substrates endowed of good plasmonic functionalities and low detection limits in ligand-free conditions, i.e. no stabilizing agents that hinder the detection capabilities. Our fabrication process of transparent plasmonic devices combines different concepts including laser lithography for glass microstructuring[40-43], laser synthesis of ligand-free nanoparticles in solution phase[44-52] and their assembly by a hydrophobic surface-based strategy[53, 54]. Briefly, the mask-projection technique provides a prompt (<1 second) surface irradiation inducing photochemical modification in the glass, being a prerequisite for the fabrication of hydrophobic and transparent, large-area conical patterns. As to be explained thereafter, the hydrophobic surface enables the accurate control of spatial distribution and delivery of ligand-free Au NPs to the surface area (tip of the cones). This approach strongly improves the detection limit with a cleaner signal by reducing the active area of the sensor and chemical effects (bare and clean surface of Au NPs)[37], moreover, it can be extended to large-area processing for mass production. Therefore, the proposed approach can help to overcome all limitations introduced above. The detection efficiency, i.e., the SERS enhancement factor, can be evaluated by using cresyl violet (CV) molecules. The SERS signal results enhanced of three orders of magnitude compared to other SERS-sensitized metallic surfaces.

[a] *Nanophysics, Istituto Italiano di Tecnologia, via Morego, 30, 16163 Genova, Italy. E-mail corresponding author: romuald.intartaglia@iit.it,*

[b] *Nanostructure, Istituto Italiano di Tecnologia, via Morego, 30, 16163 Genova, Italy.*

† Electronic supplementary information (ESI) available. See DOI

As we report below, the transparent SERS device is able to detect CV molecules at an estimated level of 1 nM within only 100 ms of integration time and very low laser power (55 μW). The collected data suggest that for longer integration time, higher laser power and further optimization, the detection limit far below the picomolar range can be achieved.

Results and discussions

Laser fabrication of large-area hydrophobic microtip array

The fabrication of large-area microtip arrays on biocompatible glass is performed in three steps (laser irradiation, annealing, wet etching). To increase the microtip surface area, only the first step, i.e. the laser irradiation, has to be scaled up and extended to a larger area by applying a step-and-repeat method for high-throughput production. For instance, an area of 5 x 5 cm^2 would be irradiated in less than 30 seconds. The subsequent annealing and etching steps take about 5 and 0.5 hours, respectively. The time needed for these last two steps don't depend on the size of the device. In the first step, excimer laser irradiation of photosensitive glass is applied using mask projection technique to write latent images/patterns in the glass. The size of the device discussed in the manuscript has a 5 mm-diameter area (see figure 1e) and the size can be scaled up to several cm^2 by using multiple laser irradiations in the XY plane and/or increasing the laser spot size of the mask-projection system (see Figure 1Sa). Experiments were carried out using a KrF excimer laser operating at 248 nm with pulse duration of 20 ns and a laser fluence of 0.2 J cm^{-2}, coupled with a micromachining workstation (Micromaster, Optec). A single laser pulse was fired on the glass surface. For mask patterns, lithographic photomasks (chromium on quartz) are used with a pattern corresponding to the desired 3-D geometry to be fabricated in the glass. The resulting latent image in the glass forms a pattern where the center-to-center (center means the final fabricated microtip) distance is determined by the distance “d” on the mask divided by 4 due to the 4x demagnification of the mask projection system (Figure 2S). The second step consists of annealing the glass sample in a programmable furnace for the formation of crystalline phase of lithium metasilicate. The temperature is first ramped up to 500 °C at 5 °C/min, held at this temperature for 1 h, then rose to 605 °C at a rate of 3 °C/min, and held for another hour. In the third step (Figure 1) the glass chip is immersed in an aqueous solution of 10 % hydrofluoric acid (HF) in ultrasonic bath for the selective removal of the laser-exposed zone. During this last process an intense etching starts on the laser-exposed region, but at the same time, the unexposed glass surface is also etched. In other words, the etching process promptly starts on the whole glass surface indicated by yellow arrows in Figure 1a. The thinner yellow arrows represent a slower etching rate to which the non laser-exposed glass surface is subjected. The conical array formation, demonstrated in Fig. 1a-c, is a consequence of different etching periods at different depths inside the glass, i.e., the glass surface on the top is exposed to a longer etching time than the deeper regions, resulting in the formation of conical tips between the laser-exposed zones (Figure 1c). Microtip arrays with desired geometry and aspect ratios can be realized through the highly time-dependent and accurate etching process. SEM images of conical arrays with different aspect ratios on the glass surface obtained at different etching time from 10 to 25 minutes are shown in Figure 1f-j. The appropriate etching conditions are thus crucial for the desired microtip formation. Figure 2S show other embedded structures in glass pointing out to the versatility and easy realization of the mask-projection technique. As it is well known, the surface roughness allows to control the wettability properties.

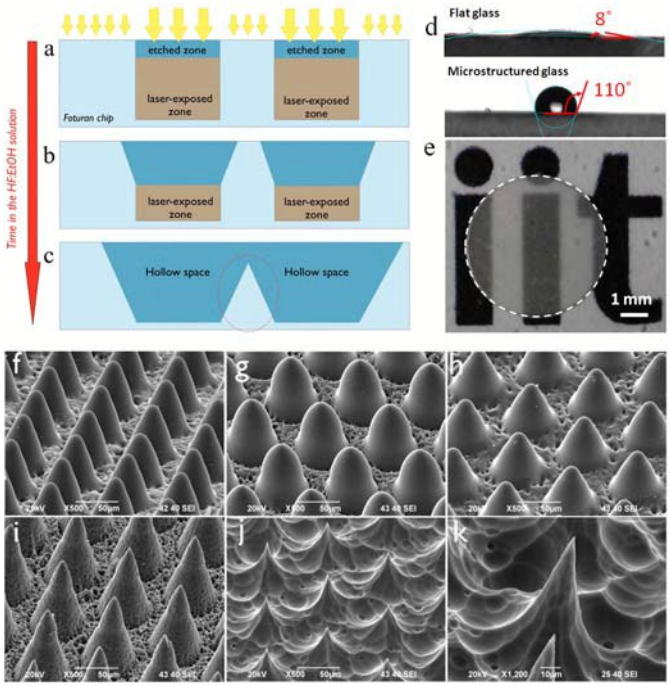

Figure 1: a-c) Schematic representation of the chemical etching process on the previously laser-exposed and annealed glass chip, i.e., the microtip array formation. d) presents the modification of the wettability behavior of the glass surface. The contact angle changes from 8° to 110° due to laser surface microstructuring. Image e) shows an optical microscopy image of laser-treated glass surface (dashed circle) confirming the preserved transparency of the substrate. The microstructured surface within the dashed circle is presented in Figure k). Images (f-k) display various conical structures when using the same mask, but different chemical etching periods, 5, 10, 15, 20, 25, 30 minutes respectively. These f-k) images highlight the importance of the etching process being a crucial experimental step to achieve the desired geometry, height, and aspect ratios.

In the present case, the obtained conical surface microstructuring turns the surface wetting properties from hydrophilic to hydrophobic as demonstrated in Figure 1d. The contact angle measurements show an increase from a value of 8° (on water-flat glass) to 110° (on microstructured glass). Note that hydrophobic surfaces obtained by our method are reproducible and can be scaled up by multiple folds if applying a step-and-repeat method for high-throughput production. Moreover, as shown in Figure 1e, the transparency of the laser-treated glass surface with a 5 mm diameter (dashed circle) is preserved.

Self-localization of ligand-free Au nanoparticles on hydrophobic microstructured transparent surface

The realisation of the hydrophobic surface is a key point in the self-localization process of NPs and molecules dissolved in solution. In fact, it enables the self-positioning of ligand-free NPs or molecules dissolved in aqueous solution.[53, 54] Recently, Yang et al reported that analyte molecules could be significantly enriched by using the superhydrophobic surface properties before SERS detection, enabling an extremely sensitive detection of molecules in a highly diluted solution.[55] The deposition method is the following: a drop of water containing ligand-free Au NPs is deposited onto the microstructured hydrophobic glass, (Figure 2A). The low adhesion

force between the drop, i.e., liquid sample of Au NPs and the microstructured glass surface allows the drop to evaporate, while shrinking in volume and maintaining its quasi-spherical shape. During the evaporation of the solution of ligand-free Au NPs, the particles become more and more concentrated. At the end of the process, when the shape and concentration reach an unstable condition, the drop collapses and the ligand-free NPs are deposited on the top of microtips. This procedure can be automatized by employing inkjet printers which, when properly optimized, can allow quasi-uniform coverage (by overlapping spotting points) over a large area. For the proof of concept of a plasmonic device fabrication, we employed a laser-treated surface displaying hydrophobic properties with 110˚, as shown in figure 1e. In figure 2B-D are presented SEM images of laser fabricated hydrophobic microtip array after the NPs self-positioning process with three magnifications: overview of the 5 mm processed area (figure 3B), close-up of the microtip array displaying homogeneous, periodic and conical microstructure (figure 3C) and single microtip with a sub-100 nm-sized tip coated with ligand-free Au NPs (figure 3D). As we report below, Raman analysis of several randomly selected microtips coated with ligand-free Au NPs confirmed the presence and uniformity of nanoparticles over the microstructured area. On the other hand, the sub-100 nm-sized tip together with ligand-free Au NPs is the key point for good plasmonic functionalities, as discussed in the next section. Ligand-free Au-NPs prepared by femtosecond laser ablation of a gold target in deionized water are reported in figure 2D. In the inset of the histogram the NP size distribution is shown, obtained by counting the particles in the electron microscopy image. Isolated 8-nm ligand-free Au NPs with a pseudo-spherical morphology and a smooth surface are obtained displaying a plasmon resonance peak at around 520 nm (see also method section and Figure 3S). The feasibility of using a hydrophobic surface-based self-positioning method to assemble the Au NPs onto the top of a conical transparent microstructure is supported by optical analysis. One can note that the positioning of ligand-free Au NPs on the top of conical microtips allows to preserve the transparent properties of plasmonic devices. The total transmission spectra of a flat glass substrate (red line), microstructured glass (blue line), and conical glass microtip coated with Au-NPs (black line) are presented in Figure 3. The Au NPs-coated microstructured glass-based plasmonic device displays highly transparent properties in the visible spectral range. Due to the scattering of the microtip arrays, the transmittance of the microstructured glass is lower than the original glass. Additionally, the dip observed at 540 nm represents the plasmon resonance of the Au NPs deposited on the top of conical microtips confirming the presence of Au NPs on the conical microtip. This characteristic plasmonic feature can be compared with the scattering spectra of similar Au NPs arrays deposited randomly on glass substrates recently published.[56] On the right side of figure 3, the optical microscopy image in transmission mode of human hair deposited on plasmonic device is shown. Cellulose fiber deposited on the substrate showcasing the potentiality of the plasmonic device for multimodal optical analysis, i.e. visualization and characterization is presented in Fig.5S.

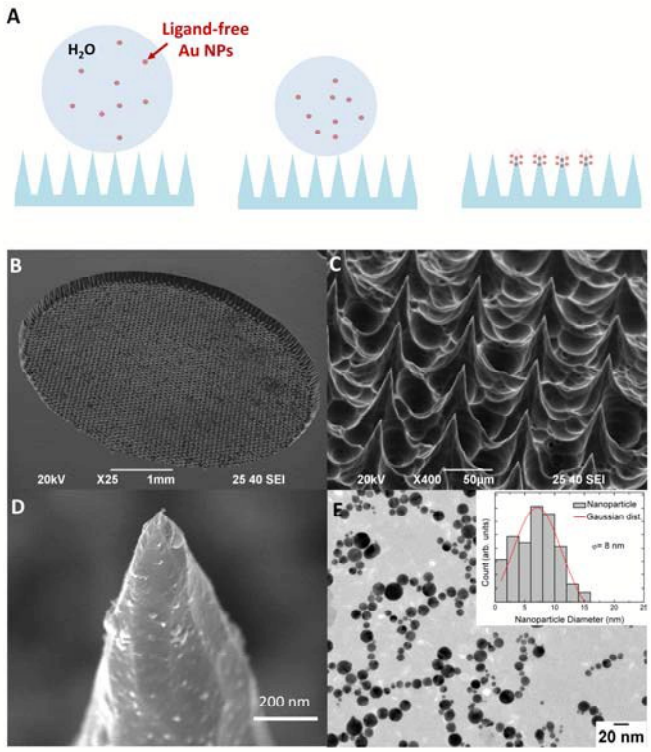

Figure 2. A) Scheme (not in scale) of drop evaporation on the hydrophobic and transparent surface delivering ligand-free Au NPs to the top of the microtip. SEM images showing the plasmonic microtip sensor array with three magnifications: B) overview of the 5 mm processed area C) close-up of the microtip array, D) Single microtip with a sub-100 nm-sized tip coated with ligand-free Au NPs. E) TEM image of ligand-free Au-NPs prepared by ultrafast pulsed laser ablation in deionized water.

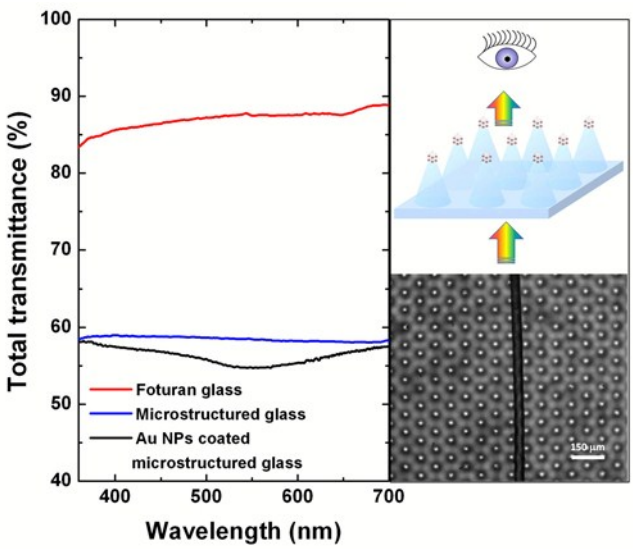

Figure 3. Total transmittance spectra of a flat glass (red line), a microstructured glass (blue line), and Au NPs-coated microstructured glass (black line). On the right side, an optical microscopy image in transmission mode of a human hair deposited on the plasmonic device is shown.

Plasmonic features and SERS analyses

The ligand-free Au NPs are anchored by adhesion forces. Once they are delivered they will remain stuck to the surface even when another drop of solution is deposited on the sample. Therefore, the self-positioning process can be repeated again to deliver analytes in the same area where Au NPs are located. This approach strongly improves the detection limit because it reduces the active area of the sensor (thus reducing the background noise) and it allows to deliver all molecules exclusively to the plasmonic active area, even when highly diluted samples are investigated.[55] We notice, that in principle, other spectroscopic methods can also be used to detect the liquid sample, such as Infrared Absorption Spectroscopy, Fluorescence, Mass Spectrometry (MALDI) or others. We remark that the protocol is of general validity and in principle also other kinds of NPs can be delivered. However, ligand-free Au NPs represents a successful alternative to the conventional chemically synthesized Au NPs as revealed by detailed Raman studies (Figure 4S). Ligand-free metallic NPs display featureless Raman background spectrum (intensity is negligible), while chemically synthesized NPs with artificial ligand on NPs surface present strong Raman background signal, and thus limits the signal-to-noise ratio (Figure 4S). Consequently, the ligand-free surface of metallic NPs prepared by laser processing increase possibilities for the adsorption/immobilization of molecules and SERS detection by i) the absence of ligands at the surface of NPs which makes the NP surface available to adsorb analytes ii) reducing the artificial ligand induced vibrations effects, making SERS signals more sensitive and cleaner. The potential of this approach in terms of detection sensitivity was evaluated by using cresyl violet (CV) molecules from water solutions below the concentration of 1 nM. A drop of solution was deposited on three distinct surfaces for comparison of detection signals: 1) sputtered Au thin film on the flat glass substrate (thickness: 25 nm, reference sample C) 2) sputtered Au thin film on glass microtip (thickness: 25 nm, sample B), 3) ligand-free Au NPs anchored on a glass microtip (mean size NP: 8 nm, sample A). As a control, ligand-free Au NPs were deposited on flat glass substrate. As expected, ligand-free Au NPs were randomly distributed on the glass surface, thus limiting the sensing analysis protocol (data not shown). SERS activity of transparent plasmonic device was investigated by means of a Renishaw InVia Raman microscope with an objective of 150X (NA - 0.90) at room temperature. The spectra were recorded in backscattering geometry by irradiating it at a wavelength of 633 nm with a maximum power of 55 μW and an acquisition time of 100 ms unless mentioned otherwise. The Raman measurement performed on reference sample C chemisorbed with CV molecules (Figure 4a) shows a very low intensity Raman band centered at around 592 cm^{-1} even when a very long acquisition time of 50 s was employed. The intensity of this band increased when the SERS measurements were performed on CV deposited over the Au-evaporated microtips (sample B) with 100 ms acquisition time, showing as well the appearance of various characteristic bands of CV molecules. This increase in the SERS signal intensity is associated with an electric field enhancement due to the presence of the microtip structure.[57] In general, the smaller the tip the higher is the electric field enhancement.[58] Further increase in Raman bands' intensity throughout the spectral range was well observed for the microtip device anchored with ligand-free Au-NPs (sample A), again with 100 ms of acquisition time. This increase is associated to microtips affecting the wettability and the evaporation process, thus influencing the co-localization of nanoparticles, i.e. a higher electric field induced by the closely packed Au-NPs[59], and analyte molecules. The co-localization of nanoparticles and analyte molecules by using the hydrophobic surface properties before SERS detection enables an extremely sensitive detection of molecules in a highly diluted solution.[55] These SERS measurements indicate that the amine group of CV (-N-H_2) is attached or is in the vicinity of the Au-NPs surface leading to the appearance of the strong Raman scattering. The variation of different bands centered at 592, 674, and 1184 cm^{-1} is shown in Figure 4b. Raman analysis has been performed on several randomly selected microtips. The resulting SERS signals showed intensities with the same order of magnitudes.

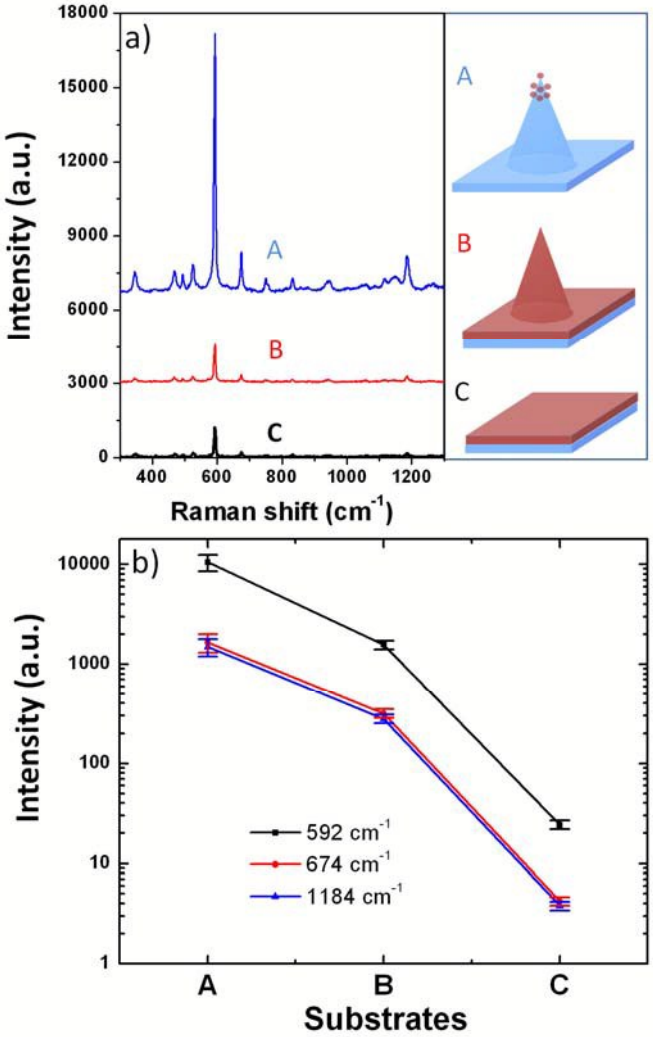

Figure 4. a) Comparison of Raman spectra with different enhancement substrates: i) ligand-free Au NPs anchored on a microtip (Scheme A, blue line). ii) Sputtered rough gold film on glass microtip (Scheme B, red line) iii) Sputtered rough gold film on the glass substrate, reference sample (Scheme C, black line). The detection is evaluated using 1 nM cresyl violet (CV) molecules. The spectra are averaged over several measurements each (λ_{ex}= 633 nm, laser power ~ 55 μW, integration time: 50 s, 0.1 s and 0.1 s respectively). b) SERS intensity of the CV characteristic vibrational band when the molecule is deposited over different substrates (laser power: 55 μW, integration time normalized to 0.1 sec). For the clarity of the figure, the Y axis is in a logarithmic scale. SERS analysis was carried out on three fabricated devices and on several randomly selected microtips over the device area, for statistical evaluation. The error bar represents the different values of the obtained SERS intensity.

Additionally, as a control, Raman analysis performed between the microtips confirm the self-localization process of NPs on the top of the microtips (Figure 6S, supporting information). These results confirm thus the presence and the uniform distribution of Au-NPs on the top of microtips over the device area. It is evident from Figure 4b that even though we don't consider the active area, i.e., number of Au-NPs where the molecules can be adsorbed, the Raman signal enhancement is of almost 3 orders of magnitude for sample A compared to the reference sample (sample C). SERS enhancement factor (EF) of Au-NPs anchored to the microtips (sample A) is estimated to be 2.5×10^5 with respect to Au-coated flat glass substrates, the reference sample (see supporting info S6). SERS EF analysis has been performed on several points, i.e. different microtips covered with ligand-free Au-NPs. The estimation of EF value depends on the active surface area, i.e. Au-NPs density per micrometer squared. One of the most characteristic parameters of a biosensing device is the detection limit. The concerned transparent SERS device is able to detect CV molecules at an estimated level of 1 nM within only 100 ms of integration time and very low laser power (55 μW). These data suggest that the detection limit can be further improved. For instance, by increasing the integration time to 10s and laser power to 0.5mW (still a reasonable time period in biosensing applications), the detection limit should reach the picomolar range without perturbation from artificial ligand surrounding NPs. In principle, by introducing additional possible optimizations (for instance, by altering the conical array density on the substrate) the degree of hydrophobicity could be changed and consequently the detection limit improve. [54, 55].

Conclusions

We have reported on a simple approach for the realization of cheap and large area hydrophobic transparent substrates endowed of good plasmonic functionalities and low detection limits in ligand-free conditions. The fabrication process is accomplished by combining i) laser lithography for glass microstructuring, ii) laser synthesis of ligand-free Au nanoparticles in solution phase, iii) and hydrophobic surface-based strategy. Hydrophobic and transparent surfaces with a large area are achieved with homogeneous conical microstructures using our mask projection and etching process approaches. The transparent plasmonic device is obtained by dropping a solution of ligand-free Au nanoparticles on the hydrophobic surface which are automatically delivered (self-localization) to the top of the micro-tips. Our approach emulates other nanoparticle self-localization methods which are costly and more cumbersome to apply and able to deliver analytes only to one single location[54]. In fact, it strongly improves the detection limit (in the picomolar range) because 1) it reduces the active area of the sensor, 2) it avoids chemical effects thus reducing the background noise due to bare and clean surface of ligand-free Au NPs, 3) it allows to deliver all analytes to the active plasmonic area (coated with Au NPs) and it can be scaled up by multiple folds by applying a step-and-repeat method for high-throughput production. We believe that the findings presented here will aid the design of future 3D transparent plasmonic devices as well as disclose the route for several SERS applications for mass production, such as *in situ* and online multimodal optical analysis in the biomedical/analytical, biology of cell membranes and surfaces, and microfluidics.

Materials and Methods

Laser synthesis of ligand-free Au nanoparticles in liquid.

The synthesis of ligand-free Au NPs was carried out by femtosecond laser ablation in an aqueous solution (deionized water) as illustrated in supplementary Figure 1Sb. The laser system used in this work consists of a Ti:Sapphire laser with a pulse width of 110 fs centered at 800 nm operating at a repetition rate of 1 kHz. The laser beam is focused using a lens with a focal length of 10 cm onto the Au target (99.999% from Alpha Aesar) placed on the bottom of a quartz cuvette and immersed in 1 ml of liquid medium, deionized water. Before each experiment, the target was mechanically polished and then washed several times with the same liquid used for the ablation to remove the impurity from the surface. During the laser ablation, the target was moved with a rotation system (T-cube DC Servo controller, Thor labs) to achieve uniform irradiation of the gold surface.

NPs and plasmonic Characterization

The determination of size and size distribution of the Au NPs was performed by Transmission electron microscopy (TEM) imaging with a JEOL Jem 1011 microscope working at an acceleration voltage of 100 KeV. One drop of the suspension was deposited directly onto carbon-coated 300 mesh copper grid leaving the solvent to evaporate. Scanning electron microscopy (SEM) using a JEOL JSM-6490 electron microscope was employed for characterization of the samples. The total transmittance spectra were obtained by a double beam spectrophotometer (Cary 6000i Varian) with an integrating sphere, in the range of 400-700 nm.

References

1. J. N. Anker, W. P. Hall, O. Lyandres, N. C. Shah, J. Zhao and R. P. Van Duyne, *Nature Materials*, 2008, 7, 442-453.
2. H. A. Atwater and A. Polman, *Nature Materials*, 2010, 9, 205-213.
3. D. Qu, F. Liu, J. Yu, W. Xie, Q. Xu, X. Li and Y. Huang, *Applied Physics Letters*, 2011, 98.
4. Y. Xia and N. J. Halas, *MRS Bulletin*, 2005, 30, 338-343.
5. M. C. Daniel and D. Astruc, *Chemical Reviews*, 2004, 104, 293-346.
6. S. Schultz, D. R. Smith, J. J. Mock and D. A. Schultz, *Proceedings of the National Academy of Sciences*, 2000, 97, 996-1001.
7. J. M. Nam, C. S. Thaxton and C. A. Mirkin, *Science*, 2003, 301, 1884-1886.
8. J. Yguerabide and E. E. Yguerabide, *Analytical Biochemistry*, 1998, 262, 137-156.
9. C. R. Yonzon, D. A. Stuart, X. Zhang, A. D. McFarland, C. L. Haynes and R. P. Van Duyne, *Talanta*, 2005, 67, 438-448.
10. A. J. Haes, L. Chang, W. L. Klein and R. P. Van Duyne, *Journal of the American Chemical Society*, 2005, 127, 2264-2271.
11. A. B. Dahlin, J. O. Tegenfeldt and F. Hǒǒk, *Analytical Chemistry*, 2006, 78, 4416-4423.
12. A. D. McFarland and R. P. Van Duyne, *Nano Letters*, 2003, 3, 1057-1062.
13. R. Elghanian, J. J. Storhoff, R. C. Mucic, R. L. Letsinger and C. A. Mirkin, *Science*, 1997, 277, 1078-1081.
14. G. Raschke, S. Kowarik, T. Franzl, C. Sönnichsen, T. A. Klar, J. Feldmann, A. Nichtl and K. Kürzinger, *Nano Letters*, 2003, 3, 935-938.
15. C. L. Haynes, C. R. Yonzon, X. Zhang and R. P. Van Duyne, *Journal of Raman Spectroscopy*, 2005, 36, 471-484.
16. J. A. Dieringer, A. D. McFarland, N. C. Shah, D. A. Stuart, A. V. Whitney, C. R. Yonzon, M. A. Young, X. Zhang and R. P. Van Duyne, *Faraday Discussions*, 2006, 132, 9-26.
17. K. L. Haller, L. A. Bumm, R. I. Aitkorn, E. J. Zeman, G. C. Schatz and R. P. Van Duyne, *The Journal of Chemical Physics*, 1989, 90, 1237-1252.
18. W. H. Yang, J. Hulteen, G. C. Schatz and R. P. Van Duyne, *Journal of Chemical Physics*, 1996, 104, 4313-4323.
19. T. R. Jensen, R. P. Van Duyne, S. A. Johnson and V. A. Maroni, *Applied Spectroscopy*, 2000, 54, 371-377.
20. M. Moskovits, *Reviews of Modern Physics*, 1985, 57, 783-826.
21. K. Aslan, J. R. Lakowicz, H. Szmacinski and C. D. Geddes, *Journal of Fluorescence*, 2005, 15, 37-40.

22. Y. Chen, K. Munechika and D. S. Ginger, *Nano Letters*, 2007, 7, 690-696.
23. P. D. O'Neal, G. L. Coté, M. Motamedi, J. Chen and W. C. Lin, *Journal of Biomedical Optics*, 2003, 8, 33-39.
24. R. Sulk, C. Chan, J. Guicheteau, C. Gomez, J. B. B. Heyns, R. Corcoran and K. Carron, *Journal of Raman Spectroscopy*, 1999, 30, 853-859.
25. L. Wang, T. Li, Y. Du, C. Chen, B. Li, M. Zhou and S. Dong, *Biosensors and Bioelectronics*, 2010, 25, 2622-2626.
26. E. C. Le Ru, P. G. Etchegoin, J. Grand, N. Félidj, J. Aubard, G. Lévi, A. Hohenau and J. R. Krenn, *Current Applied Physics*, 2008, 8, 467-470.
27. G. Das, F. Mecarini, F. Gentile, F. De Angelis, H. G. Mohan Kumar, P. Candeloro, C. Liberale, G. Cuda and E. Di Fabrizio, *Biosensors and Bioelectronics*, 2009, 24, 1693-1699.
28. M. G. Banaee and K. B. Crozier, *Optics Letters*, 2010, 35, 760-762.
29. N. M. B. Perney, J. J. Baumberg, M. E. Zoorob, M. D. B. Charlton, S. Mahnkopf and C. M. Netti, *Opt. Express*, 2006, 14, 847-857.
30. A. Hamdorf, M. Olson, C.-H. Lin, L. Jiang, J. Zhou, H. Xiao and H.-L. Tsai, *Opt. Lett.*, 2011, 36, 3353-3355.
31. M. J. Beliatis, S. J. Henley and S. R. P. Silva, *Opt. Lett.*, 2011, 36, 1362-1364.
32. L. Su, T. H. Lee and S. R. Elliott, *Opt. Lett.*, 2009, 34, 2685-2687.
33. C.-H. Lin, L. Jiang, Y.-H. Chai, H. Xiao, S.-J. Chen and H.-L. Tsai, *Opt. Express*, 2009, 17, 21581-21589.
34. C.-H. Lin, L. Jiang, J. Zhou, H. Xiao, S.-J. Chen and H.-L. Tsai, *Opt. Lett.*, 2010, 35, 941-943.
35. S. K. Yang, W. P. Cai, L. C. Kong and Y. Lei, *Adv Funct Mater*, 2010, 20, 2527-2533.
36. K. C. Grabar, R. G. Freeman, M. B. Hommer and M. J. Natan, *Analytical Chemistry*, 1995, 67, 735-743.
37. R. Intartaglia, G. Das, K. Bagga, A. Gopalakrishnan, A. Genovese, M. Povia, E. Di Fabrizio, R. Cingolani, A. Diaspro and F. Brandi, *Physical Chemistry Chemical Physics*, 2013, 15, 3075-3082.
38. J. P. Singh, T. E. Lanier, H. Zhu, W. M. Dennis, R. A. Tripp and Y. Zhao, *The Journal of Physical Chemistry C*, 2012, 116, 20550-20557.
39. H.-H. Wang, T.-Y. Cheng, P. Sharma, F.-Y. Chiang, S. W.-Y. Chiu, J.-K. Wang and Y.-L. Wang, *Nanotechnology*, 2011, 22, 385702.
40. S. Beke, L. Korösi, K. Sugioka and K. Midorikawa, *Journal of Laser Micro Nanoengineering*, 2012, 7, 28-32.
41. S. Beke, L. Korösi, K. Sugioka, K. Midorikawa and I. Dékány, *Applied Physics A: Materials Science and Processing*, 2011, 102, 265-269.
42. K. Sugioka, M. Masuda, T. Hongo, Y. Cheng, K. Shihoyama and K. Midorikawa, *Applied Physics A: Materials Science and Processing*, 2004, 79, 815-817.
43. S. Beke, F. Anjum, L. Ceseracciu, I. Romano, A. Athanassiou, A. Diaspro and F. Brandi, *Laser Physics*, 2013, 23, 035602.
44. R. Intartaglia, K. Bagga, F. Brandi, G. Das, A. Genovese, E. Di Fabrizio and A. Diaspro, *The Journal of Physical Chemistry C*, 2011, 115, 5102-5107.
45. R. Intartaglia, A. Barchanski, K. Bagga, A. Genovese, G. Das, P. Wagener, E. Di Fabrizio, A. Diaspro, F. Brandi and S. Barcikowski, *Nanoscale*, 2012, 4, 1271-1274.
46. K. Bagga, A. Barchanski, R. Intartaglia, S. Dante, R. Marotta, A. Diaspro, C. L. Sajti and F. Brandi, *Laser Physics Letters*, 2013, 10.
47. R. Intartaglia, K. Bagga, A. Genovese, A. Athanassiou, R. Cingolani, A. Diaspro and F. Brandi, *Physical Chemistry Chemical Physics*, 2012, 14, 15406-15411.
48. D. M. Popovic, J. S. Chai, A. A. Zekic, M. Trtica, M. Momcilovic and S. Maletic, *Laser Physics Letters*, 2013, 10.
49. F. Hajiesmaeilbaigi, A. Mohammadalipour, J. Sabbaghzadeh, S. Hoseinkhani and H. R. Fallah, *Laser Physics Letters*, 2006, 3, 252-256.
50. S. Z. Mortazavi, P. Parvin and A. Reyhani, *Laser Physics Letters*, 2012, 9, 547-552.
51. R. Intartaglia, K. Bagga and F. Brandi, *Optics Express*, 2014, 22, 3117-3127.
52. R. Intartaglia, K. Bagga, M. Scotto, A. Diaspro and F. Brandi, *Opt. Mater. Express*, 2012, 2, 510-518.
53. E. Miele, M. Malerba, M. Dipalo, E. Rondanina, A. Toma and F. D. Angelis, *Advanced Materials*, 2014, DOI: 10.1002/adma.201400310, n/a-n/a.
54. F. De Angelis, F. Gentile, F. Mecarini, G. Das, M. Moretti, P. Candeloro, M. L. Coluccio, G. Cojoc, A. Accardo, C. Liberale, R. P. Zaccaria, G. Perozziello, L. Tirinato, A. Toma, G. Cuda, R. Cingolani and E. Di Fabrizio, *Nat Photonics*, 2011, 5, 683-688.
55. S. K. Yang, P. J. Hricko, P. H. Huang, S. X. Li, Y. H. Zhao, Y. L. Xie, F. Guo, L. Wang and T. J. Huang, *J Mater Chem C*, 2014, 2, 542-547.
56. D. Gaspar, A. C. Pimentel, T. Mateus, J. P. Leitao, J. Soares, B. P. Falcao, A. Araujo, A. Vicente, S. A. Filonovich, H. Aguas, R. Martins and I. Ferreira, *Sci Rep-Uk*, 2013, 3.
57. F. De Angelis, C. Liberale, M. L. Coluccio, G. Cojoc and E. Di Fabrizio, *Nanoscale*, 2011, 3, 2689-2696.
58. R. P. Zaccaria, F. De Angelis, A. Toma, L. Razzari, A. Alabastri, G. Das, C. Liberale and E. Di Fabrizio, *Optics Letters*, 2012, 37, 545-547.
59. F. De Angelis, G. Das, P. Candeloro, M. Patrini, M. Galli, A. Bek, M. Lazzarino, I. Maksymov, C. Liberale, L. C. Andreani and E. Di Fabrizio, *Nat Nanotechnol*, 2010, 5, 67-72.

.

